CFD analysis of the airflow behavior in the intake system of a low-displacement diesel engine

Análisis CFD del comportamiento del flujo de aire en el sistema de admisión de un motor diésel de baja cilindrada

DOI: http://doi.org/10.17981/ingecuc.16.2.2020.23

Artículo de Investigación Científica. Fecha de Recepción: 20/12/2019. Fecha de Aceptación: 22/10/2020.

Carlos Santos
Universidad del Atlántico. Barranquilla (Colombia)
cesantos@mail.uniatlantico.edu.co

Luis Pérez
Universidad del Atlántico. Barranquilla (Colombia)
luismiguelperez@mail.uniatlantico.edu.co

Jorge Duarte Forero
Universidad del Atlántico. Barranquilla (Colombia)
jorgeduarte@mail.uniatlantico.edu.co

Para citar este artículo:
C. Santos, L. Pérez & J. Duarte Forero, "CFD analysis of the airflow behavior in the intake system of a low-displacement diesel engine", *INGE CUC*, vol. 16, no. 2, pp. 285–298. DOI: http://doi.org/10.17981/ingecuc.16.2.2020.23

Abstract

Introduction— The airflow analysis for Internal Combustion Engines (ICE) remains challenging for researchers due to the complexity of the flow interactions inside the cylinder. Different flow characteristics such as turbulence, instability, periodicity, and non-stationary conditions required advanced methods to describe the overall behavior. The present study proposed the implementation of a turbulence model through Computational Fluid Dynamics (CFD) analysis that further simplifies the airflow phenomena for low-displacement engines while describing the parameters that influence the engine efficiency and emissions.

Objectives— The study aims to analyze the airflow behavior in the intake system of a low-displacement diesel engine with natural aspiration through an experimental model adjusted by CFD analysis.

Methodology— The analysis of the airflow behavior in the intake system of the engine was carried out with an experimental model that describes the airflow characteristics. This model is adjusted via CFD analysis in OPENFOAM®, which determines Both Discharge (DC) and Swirl Coefficients (SC) to describe the flow interactions in the intake system.

Results— The DC values ranged between 0 L/D to 0.5 L/D, indicating that this engine can displace 50% of the ideal airflow with a valve diameter of 30.5 mm and a chamber volume of 0.3 L. In contrast, the SC, for a variable reference area, ranged from 0. L/D 3 to 0.19 L/D, stating that the engine experiences less airflow displacement, specifically 11% of the theoretical capacity as the mass flow increases for each valve lift.

Conclusions— In conclusion, the methodology implemented in the study showed that for rotatory regimes of 3000 rpm and 3400 rpm, a concrete vortex is generated with velocity values between 10 m/s and 20 m/s in the peripherical region, which ensures the airflow rotation with vorticity inside the cylinder. At 3400 rpm, the SC value increments are compared to other regimes when the end of the valve lift distance is reached. Thus, it can be verified that under this regime, the optimal vorticity generation is achieved, which contributes to reduce emissions and boost the global efficiency of the engine.

Keywords— Diesel engines; OpenFOAM; CFD; discharge coefficient; swirl motion

Resumen

Introducción— El análisis del flujo de aire, en Motores de Combustión Interna expone un gran desafío para los investigadores debido al comportamiento que presenta el aire dentro del cilindro, el cual se caracteriza por ser turbulento, inestable, cíclico y no estacionario tanto espacial como temporalmente. El presente estudio propone implementar de un modelo de turbulencia a través de un análisis de Dinámica de Fluidos Computacional (CFD) que permita simplificar el fenómeno para motores de baja cilindrada y describa los parámetros que repercuten en la eficiencia y emisiones del motor.

Objetivos— El presente estudio busca analizar el comportamiento del flujo de aire en el sistema de admisión de un motor Diésel de baja cilindrada con aspiración natural a través de un modelo experimental ajustado mediante un modelado CFD.

Metodología— Se realizó el análisis del comportamiento del flujo de aire en el sistema de admisión del motor con un modelo experimental que obtiene las características del flujo. Este modelo es ajustado mediante herramientas CFD en OPENFOAM®, que permitirá obtener el Coeficiente de Descarga (CD) y el Coeficiente de Torbellino (CT) para describir el comportamiento aerodinámico del sistema de admisión.

Resultados— Para el CD, los valores oscilan entre 0 L/D y 0.5 L/D indicando que este motor es capaz de trasegar un 50% de aire de la capacidad teórica con una válvula de 30.5 mm de diámetro y una cámara de 0.3 L de volumen. En cuanto al CT, para un área de referencia variable, los valores oscilan entre 0.19 L/D y 0.3 L/D, por lo que el motor solo disminuiría un 11% su capacidad de trasegar flujo de aire de la capacidad ideal, si el flujo másico teórico va en aumento para cada levantamiento.

Conclusiones— Se puede concluir que para 3000 rpm y 3400 rpm se produce un vórtice definido bajo la metodología propuesta, obteniendo valores de velocidad muy cercanos a 10 m/s y 20 m/s en la periferia, que aseguran el flujo de aire con vorticidad en el cilindro. A 3400 rpm el CT se eleva con respecto a los demás regímenes en los últimos levantamientos de válvula. Concluyendo así, que bajo este régimen de giro se da el punto óptimo de generación de vorticidad para el motor que permite reducir las emisiones e incrementar le eficiencia global.

Palabras clave— Motores Diésel; CFD; OpenFOAM; coeficiente de descarga; coeficiente de torbellino

I. Introduction

Reducing greenhouse emissions has become the main priority of thermal sciences. Diesel engines possess a significant portion of global emissions [1]. Thus, the insightful understanding and further optimization of combustion phenomena foster reliability while reducing the harmful effects of the operation. In this sense, the airflow in Internal Combustion Engines (ICE) is influenced by the admission and compression processes. During admission, the airflow inlet is completely related to the geometry patterns of the ducts and admission valves; thus, the relevance of the combustion chamber configuration is not determinant. Therefore, the study of the admission system regarding the generation of vorticity and turbulence promotes the optimization of the airflow in the chamber.

The airflow analysis in ICEs remains challenging for researchers due to the uncertainty of the overall behavior of the air inside the chamber, which involves instabilities, turbulence interactions, and non-steady flow [1], [2]. Thus, the description of this matter requires a rigorous characterization of the parameters that describe the airflow performance and subsequent influence on the compression ratio that enables control of the NOx and soot emissions. In this study, both experimental and theoretical approaches are incorporated to generate a clear perspective of airflow optimization.

The experimental model implemented was first proposed in 2007 [5]. It provides accurate emulation of the physical characteristics of the airflow phenomena through a combined methodology of representative variables and stationary flow air model that describes geometric and operational contributions of the system. For 1951 was introduced the flow air analysis of the admission system based on an experimental approach by implementing an anemometer to measure the vorticity generation [6]. Subsequently, in 1965 was developed a more complex methodology named AVL [7], which incorporates the anemometry previously described while integrated with a theoretical approach [8]. In this sense, the AVL methodology describes the airflow analysis when the admission valve is opening based on the instantaneous vorticity generation [7].

On the other hand, the theoretical models center on the mathematical characterization of the airflow process while relating experimental data and configuration patterns. Thus, the focus of this model is to parametrize the airflow model before entering the combustion chamber due to the impact on the combustion process. In fact, this study takes relevance to the spontaneous ignition of the air-fuel mixture of ICEs [5], [9]. Overall, the theoretical models can be divided into dimensional [10], non-dimensional, and quasi-dimensional models [11].

The main difference of the theoretical model mentioned yields on the velocity profile. Thereby, there is not space variation on the profile velocity in the non-dimensional model, whereas the quasi-dimensional model accounts for velocity variations of the profile velocity inside the airflow. However, the interaction of velocity profiles is neglected [4]. Lastly, the dimensional model provides a complete description of the velocity profiles as a distribution of vectors [5], [12]. The application of every model is immersed in the AVL model [13]. This method highlights for its simplicity to determine the mean angular velocity in ICEs [14]. Due to the minor complexity, this model has been extensively implemented in the characterization of the admission system while determining both flow and swirl coefficients for each valve lift.

In 1983 was implemented an experimental test model of the airflow of the combustion chamber of an ICE while determining non-dimensional parameters to describe the vorticity development in the cylinder [8], [5]. For 1974 was proposed a thermodynamic approach that separates the tangential vortex generations for the admission and compression processes [15], [5]. Accordingly, to calculate the radial airflow entering the combustion chamber, the mathematical expression proposed by IHC is used [8]. The SAE proposed a non-dimensional model [16] to determine the rotational speed of the airflow during the combustion process [5]. This incorporates a tangential velocity profile with a parabolic shape that provides an enhanced match of the compression stroke [18], [24].

The present study aims to develop a methodology that describes the behavior of the airflow patterns in the intake process of a single-cylinder diesel engine via CFD analysis. This investigation contributes to close the knowledge gap regarding the limitations of available models to describe the airflow contribution on combustion performance and emissions.

II. CFD METHODOLOGY

Due to the high volume of airflow during the intake process of ICEs, it is considered turbulent and arbitrary. Therefore, the nature of the velocity and pressure can be classified as unstable. To describe the turbulent interactions inside the combustion chamber, a CFD approach is required as it provides a complete description of the physical phenomena [19].

The CFD model incorporates the Reynolds-Averaged Navier Stokes (RANS) equations to determine the flow behavior when the heat transfer is occurring. The conventional k-ε model provides an approximated solution to the governing equations which describe the airflow within the admission process. The last model integrates the transport equations for the kinetic energy (k) and its dissipation rate (ε) to generate a robust turbulence model with reasonable computational demand to obtain convergence [20]. In fact, this turbulence model stands to be the most employable method for ICE combustion modeling, as it provides an accurate approximation of the airflow behavior [21], [22]. The fundamental equations for the model are described as follows:

$$\frac{\partial}{\partial t}(\rho k)+\frac{\partial}{\partial x_j}(\rho k u_j)=\frac{\partial}{\partial x_j}\left[\left(\mu+\frac{\mu_t}{\sigma_k}\right)\frac{\partial k}{\partial x_j}\right]+G_k+G_b-\rho\epsilon-Y_M+S_k \quad (1)$$

$$\frac{\partial}{\partial t}(\rho\varepsilon)+\frac{\partial}{\partial x_j}(\rho\varepsilon u_j)= \frac{\partial}{\partial x_j}\left[\left(\mu+\frac{\mu_t}{\sigma_\varepsilon}\right)\frac{\partial \varepsilon}{\partial x_j}\right]+\rho C_1 S_\varepsilon-\rho C_2\frac{\varepsilon^2}{k+\sqrt{v\varepsilon}}+C_1\varepsilon\frac{\varepsilon}{k}C_{3\varepsilon}G_b+S_\varepsilon \quad (2)$$

Where G_k accounts for kinetic energy generation due to the mean velocity gradients, G_b is the kinetic energy generation produced by the buoyancy effects, Y_M represents the contribution of the compressible turbulence of the fluctuating dilatation to the total dissipation rate, S_ε and S_k are internal source terms for ε and k, respectively. v represents the flow velocity while μ and ρ are the fluid viscosity and density, respectively. The model included systems constants, which are described as $C_1\varepsilon = 1.44$, $C_2 = 1.9$, $\sigma_\varepsilon = 1.0$, and $\sigma_k = 1.2$.

III. CHARACTERIZATION OF THE AIRFLOW BEHAVIOR IN THE ENGINE

The engine selected for the study corresponds to a Sokam F300A. A complete description of the airflow behavior is obtained by analyzing the main parameters that influence the physical phenomena of the admission process under steady-state conditions. Therefore, the study incorporates the Swirl Coefficient (SC) and the Discharge Coefficient (DC). The results of the CFD takes relevance as they provide both qualitative and numerical information to evaluate the valve lift distance and compare the airflow in the combustion chamber and admission valves.

A. *Discharge Coefficient (DC)*

The appropriate calculation of DC is critical within the analysis as it determines the reliability of the model. The DC specifies the ratio between the real and theoretical mass flow rates running in the cylinder. Fig. 1 presents a schematic representation of the control volume. It can be observed that the amount of theoretical mass flow (3) is directly related to the initial conditions settled upstream and downstream of the reference area. Taking into account the mass conservation, it can be stated that the flow velocity downstream remains constant, thus $\dot{m}_{theo} = \dot{m}_2$. Therefore, DC is defined by the pressure differential between the inlet and outlet zones, which is determined by the reference area (4), (5) [23], [24].

$$\dot{m}_{the} = A_{ref}\cdot N_v\cdot\frac{P_{atm}}{(R\cdot T)^{\frac{1}{2}}}\sqrt{2\frac{\gamma}{\gamma-1}\left[\left(\frac{P_r}{P_{atm}}\right)^{\frac{2}{\gamma}}-\left(\frac{P_r}{P_{atm}}\right)^{1+\frac{\gamma}{\gamma}}\right]} \quad (3)$$

$$A_{ref} = A_{valve} = \frac{\pi\cdot {D_v}^2}{4} \quad (4)$$

$$A_{ref} = A_{IVO} = \pi\cdot d_v\cdot l_v \quad (5)$$

Hence, the following expression (6) is used to calculate the DC:

$$DC = \frac{\dot{m}_{real}}{\frac{\pi \cdot {D_v}^2}{4} N_v \frac{P_{atm}}{(R \cdot T)^{\frac{1}{2}}} \sqrt{2 \frac{\gamma}{\gamma - 1} \left[\left(\frac{P_r}{P_{atm}} \right)^{\frac{2}{\gamma}} - \left(\frac{P_r}{P_{atm}} \right)^{1+\frac{\gamma}{\gamma}} \right]}} \qquad (6)$$

Where, P_{atm} represents the ambient pressure, P_r is the compression ratio and N_v relates to the discharge coefficient. R accounts for the ideal gas constant, T is the fluid temperature, and γ is the heat capacity ratio. D_v represents the head valve diameter, d_v the body diameter and l_v the valve lift. A_{IVO} accounts for the intake valve opening area and $\dot{m}_{real}$ and $\dot{m}_{the}$ relate the real and theoretical mass flow rates.

Fig. 1. Model layout for the CFD analysis of DC.
Source: Authors.

B. *Swirl Coefficient (SC)*

The SW has been analyzed at 3 000, 3 400 and 3 800 rpm. The numerical results obtained from the CFD analysis are displayed for different valve lift distance. The study incorporates a streamlined analysis that is supported by the behavior of the tangential velocity profile at different distances from the Top Dead Center (TDC).

The calculation of the SC can be obtained from different approaches due to the variety of models available such as those proposed in previus research [7], [26], [28]. The appropriate selection is key in the analysis and depends on the engine application. In this sense, considering the characteristics of the one selected, which corresponds to a low displacement engine with helicoidal pipe and single-cylinder admission, the study has been limited to steady-state conditions. From the diversity of models, the AVL [7] stands as the most suitable method as it provides reliable results for the airflow phenomena while maintaining a relatively low error margin. SC is calculated as follows (7):

$$SC_{AVL-THIEN} = \frac{2S/D}{\pi} \frac{V_t}{V_z} \qquad (7)$$

Where V_t is the tangential speed at a $D/2$ distance, V_z is the axial velocity, S accounts for the stroke of the engine, and D relates the diameter of the bore. The AVL model differs from other methods on the description of the airflow, as it assumed the forced vortex hypothesis and uniform axial velocity to describe the instantaneous vorticity parameter. As a result, it calculates the SC as a function of the real tangential and axial velocities.

C. *MeSh analysis*

The geometry domain establishes a clear similarity to the real model while considering the type and direction of the flow inside the combustion chamber. The mesh implemented in CFD analysis is based on tetrahedral cells due to the complexity of the control volume. This cell array promotes high accuracy and stability in the results. Table 1 lists the main parameters of the mesh developed.

Table 1. Mesh parameter for steady-state calculations.

Component	Cell Type	Elements
Admission duct	Tetrahedral	105×10^3
Valve	Tetrahedral	197.5×10^3
Cylinder	Tetrahedral	104×10^3

Source: Authors.

To enable control of each mesh characteristics and reduce the simulation endeavor, the mesh of each component has been created independently. The control volume is shown in Fig. 2, where the element size is set to 0.0015 mm to enhance the interface between the wall and valve.

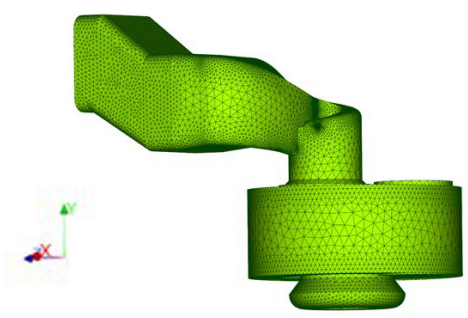

Fig. 2. Control volume mesh.
Source: Authors.

D. *Mesh Independence study*

The mesh independence study is vital for a CFD study as it guarantees the minimum number of elements required to enable stability in the calculations, which help to avoid overestimation on the computational demand that extends simulation time. The analysis selected a valve lifting distance of 2.15 mm to analyze the tangential and axial velocities and predict the SC. Fig. 3 displays the results of SC for different numbers of elements, where it can be verified that $320 \cdot 10^3$ stands as the minimal value to allow stability in the calculations. Therefore, a reasonable greater number has been selected, which is $408 \cdot 10^3$.

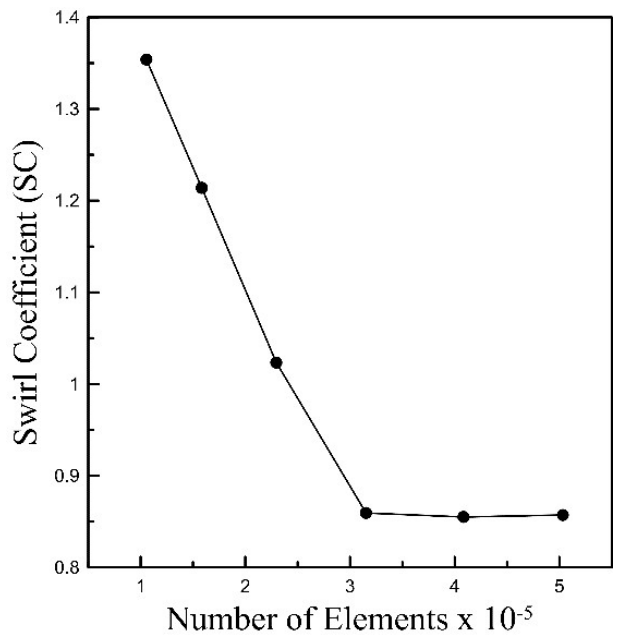

Fig. 3. Mesh independence analysis for a valve lift of 2.15 mm.
Source: Authors.

E. *Element Quality*

The quality of a mesh is measured according to the values of the asymmetry and aspect ratio in the computational domain. The comparison of the mesh implemented with the benchmarks provides a clear perspective of the overall quality of the mesh generation. Table 2 shows the characteristics values of the mesh quality in the present study, which demonstrates the appropriate patterns to compute the numerical simulations with OpenFOAM®.

TABLE 2. VALUES OF ASYMMETRY AND ASPECT RATIO.

Parameter	Asymmetry	Aspect ratio
Min	7.653×10^{-7}	1.6227×10^{-4}
Max	0.99984	0.99492
Mean	0.21304	0.78115
σ	0.12692	0.13774
Nodes	97599	
Elements	408382	

Source: Authors.

IV. CFD MODEL VALIDATION

The present study proposed a validation methodology based on previously obtained results [5] by implementing similarity laws [29], [35], [36] to extrapolate the results of the reference author with the engine used in the present study. CFD methodology stands as a robust tool to validate numerical results; indeed, it is commonly employed to redesign engines as an initial and fast technique that accounts for the thermo-fluid variables that influence the overall performance. The geometric parameters used to define both numerical and experimental models are presented in Table 3.

TABLE 3. PARAMETER OF THE ENGINE REFERENCE-MODEL AND STUDY-CASE MODEL.

0.5-1-H		Model F300A	
Admission ducts	N° of valves: 1 Duct type: Helycoidal	Admission ducts	N° of valves: 1 Duct type: Helycoidal
V_d: 0.5 L	D_v: 35.3 mm	V_d: 0.3 L	D_v: 30.5 mm
D: 80mm	l_{vmax}: 8.6 mm	D: 74.46mm	l_{vmax}: 8.6 mm
S: 93mm	r_c: 15.5	S: 62.83mm	r_c: 15.2
Natural aspiration, Direct injection, Diesel engine			

Source: Adapted [5] and manufacturer data [28].

The characteristics of the compression ratio are determined based on the manufacturer [28], and the geometric patterns were measured directly. The results of the CFD analysis for the engine F300A on a scale of 0.5 L are compared with previously obtained results [5], which are previously validated with a test bench of experimental airflow. The validation procedure can be divided into the following steps:

1) Compare the results of the intake valve opening area and the tangential velocity for the engine F300A and the engine [5] to determine the variation and similarity range.
2) Obtain a correlation for longitude (L) and volume (V) between both engines.
3) Select the correlation that makes the 0.3 L engine better match the 0.5 L engine.
4) Run the numerical simulations to obtain the intake valve opening area and the tangential velocity values.
5) Compare the results obtained from the numerical model and verify the error margin between both experimental and CFD models.

A. *Numerical simulations and validation*

The intake valve opening area and the tangential velocity measured for both engines are shown in Fig. 4a and Fig. 4b, respectively. It can be verified that the error margin of the results is not quite acceptable as they experience a concrete error propagation within the trend of the curves. The highest error margin is found on the tangential velocity distribution. However, the curve features a similar behavior as this parameter depends on whether the engine operates with one or two intake valves. Therefore, in a single-valve engine, the tangential flow behaves as a single vortex as the admission stroke begins and further maintains a constant speed until the admission ends [5], [29]. The CFD analysis will provide the

adjustment correction factor that allows obtaining reliable results between the numerical and experimental results (Fig. 5). Thus, as mentioned before, a scaled engine will be addressed through the similarity laws.

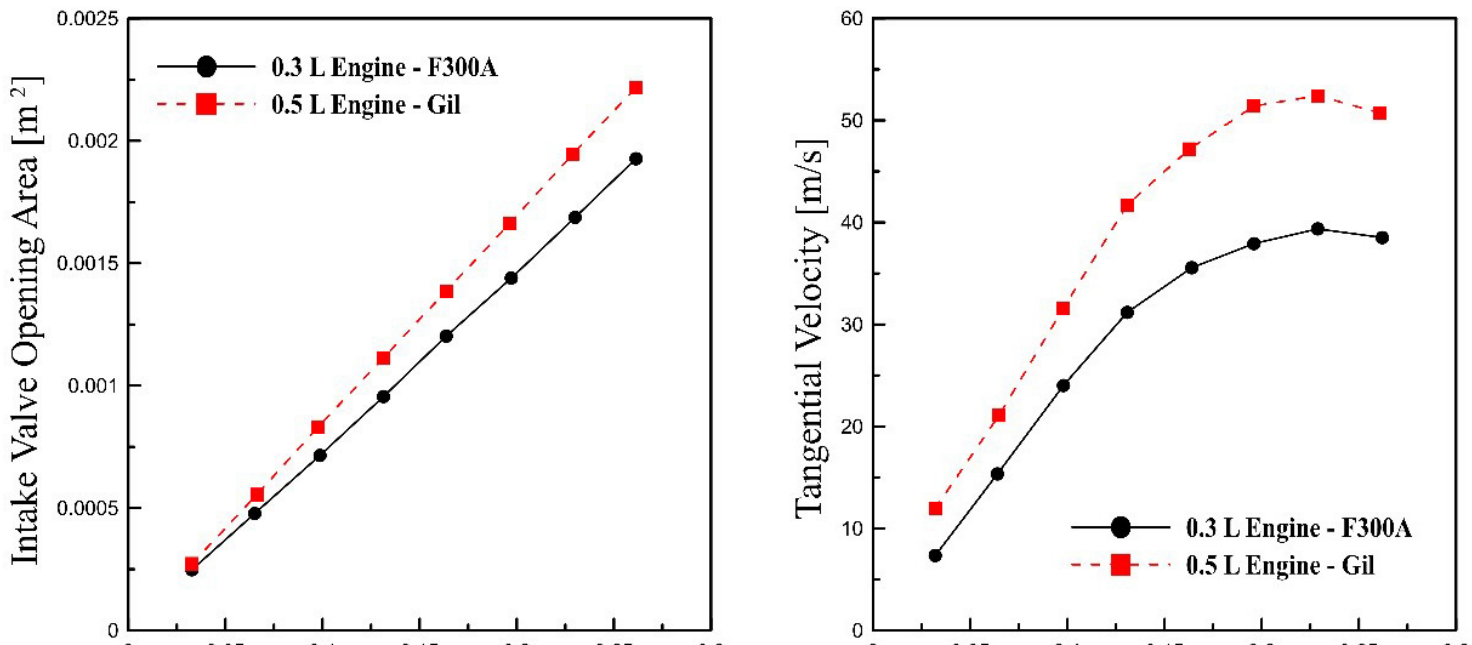

Fig. 4. Validation results of the engine reference model and study-case model. a) Intake valve opening area and b) tangential velocity.
Source: Authors.

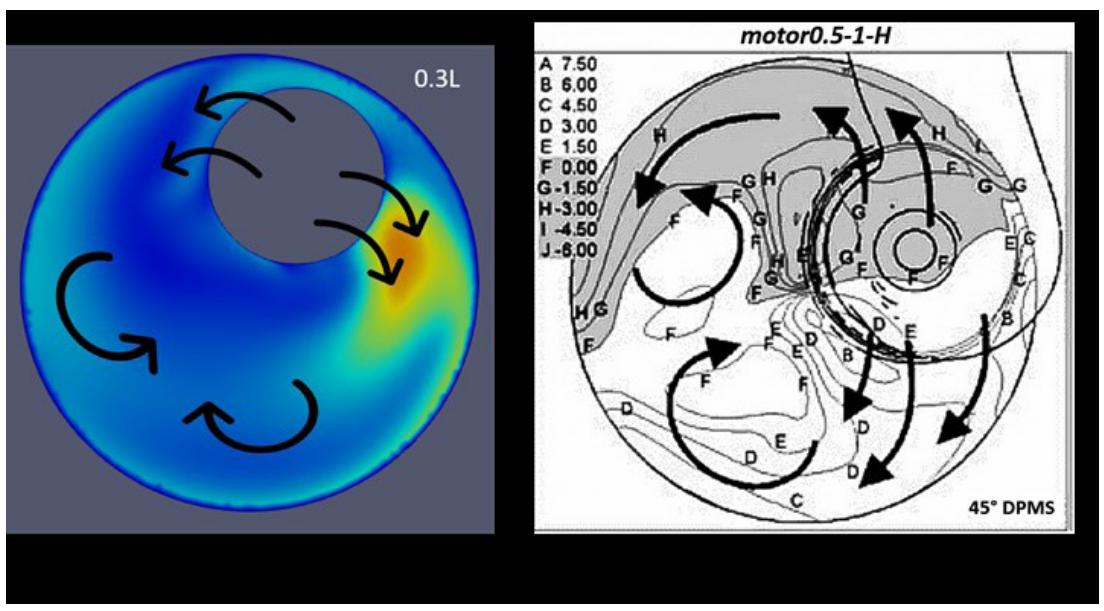

Fig. 5. Tangential velocity profiles for the first lifting of the valve for the study-model engine.
Source: Authors.

The engine that will be scaled corresponds to the F300A of 0.3 L, based on the complete characterization of the geometry patterns that allow calculating both correlations “L” and “V” designed as L = 80 mm/76.46 mm = 1.046 and V = 0.5 L/0.3 L = 1.6. The correlation of volume (V) has been selected as it helps to scale the rest of the parameters that lead to validate the model. Afterward, the similarity laws are applied based on the volume correlation and the model proposed in the study. The results are presented in Table 4, and the scaled engine characteristics are listed in Table 5.

Table 4. Values of asymmetry and aspect ratio.

Parameter	Scaled volume factor
V	$V = 1.6$
D	$V^{1/3} = 1.17$
S	$V^{1/3} = 1.17$
A	$V^{2/3} = 1.37$

Source: Authors.

TABLE 5. VALUES OF ASYMMETRY AND ASPECT RATIO.

Scaled engine F300A	
V_d = 0.5 L	D^v = 35.68 mm
D = 87.1mm	l_{vmax} = 8.6 mm
S = 73.51mm	r_c = 15.3
Natural aspiration, Direct injection, Diesel engine	

Source: Authors.

For the scaled engine F300A (experimental) under the same operating conditions of the airflow of the engine F300A of 0.3 L (present study), it was found that the relative error is not greater than 5% (Fig. 6), also the Reynolds number remains analogous (Fig. 6c) which provides equal values of turbulent intensity. In general, it can be concluded that the engine model implemented in the study with CFD correction provides appropriate results with respect to [34].

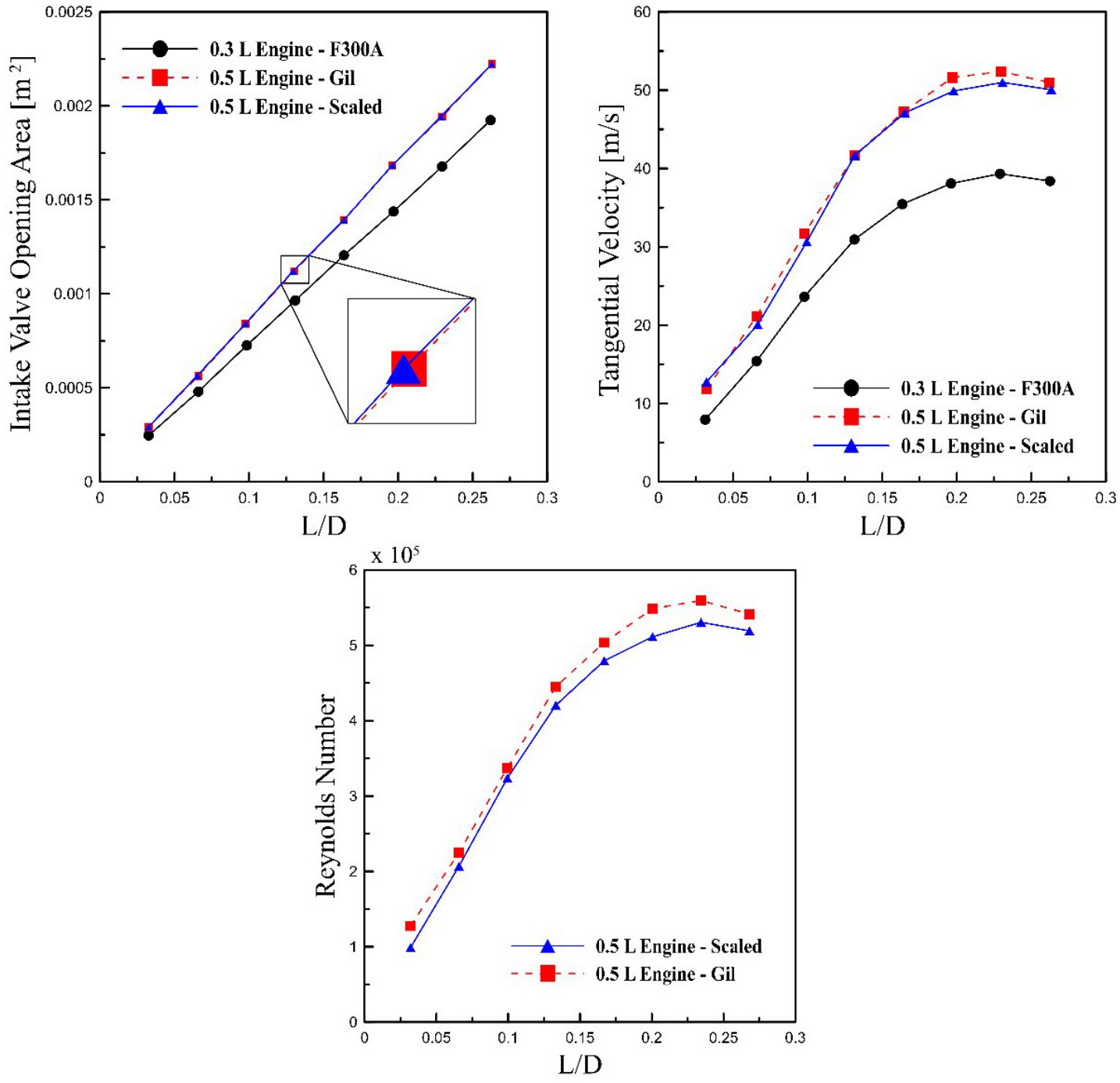

Fig. 6. Engine scaled to 0.5 L and engine without scale.
a) Intake valve opening area, tangential velocity, and (c) Reynolds number.
Source: Authors.

V. RESULTS

A. *Characterization of discharge coefficient (DC)*

The geometric differences presented in Fig. 7 expressed that the valve area is constant for all the lifting distances, whereas the intake valve opening area varies according to the shape of the cylinder as the valve moves downstream. The present study measured the DC for 8 different valve lifting distances, which generate the operation curves presented in Fig. 8.

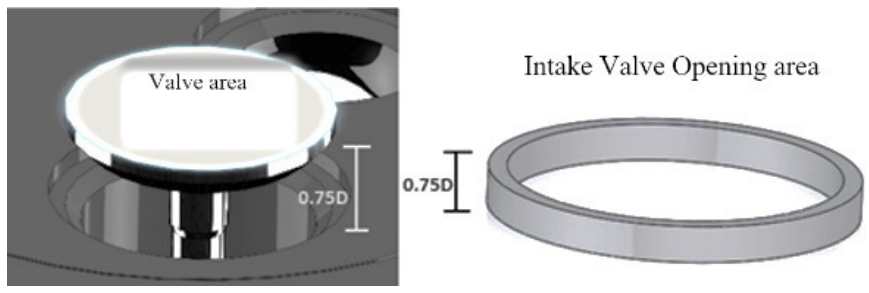

Fig. 7. Geometrical difference between valve area and gap área.
Source: Authors.

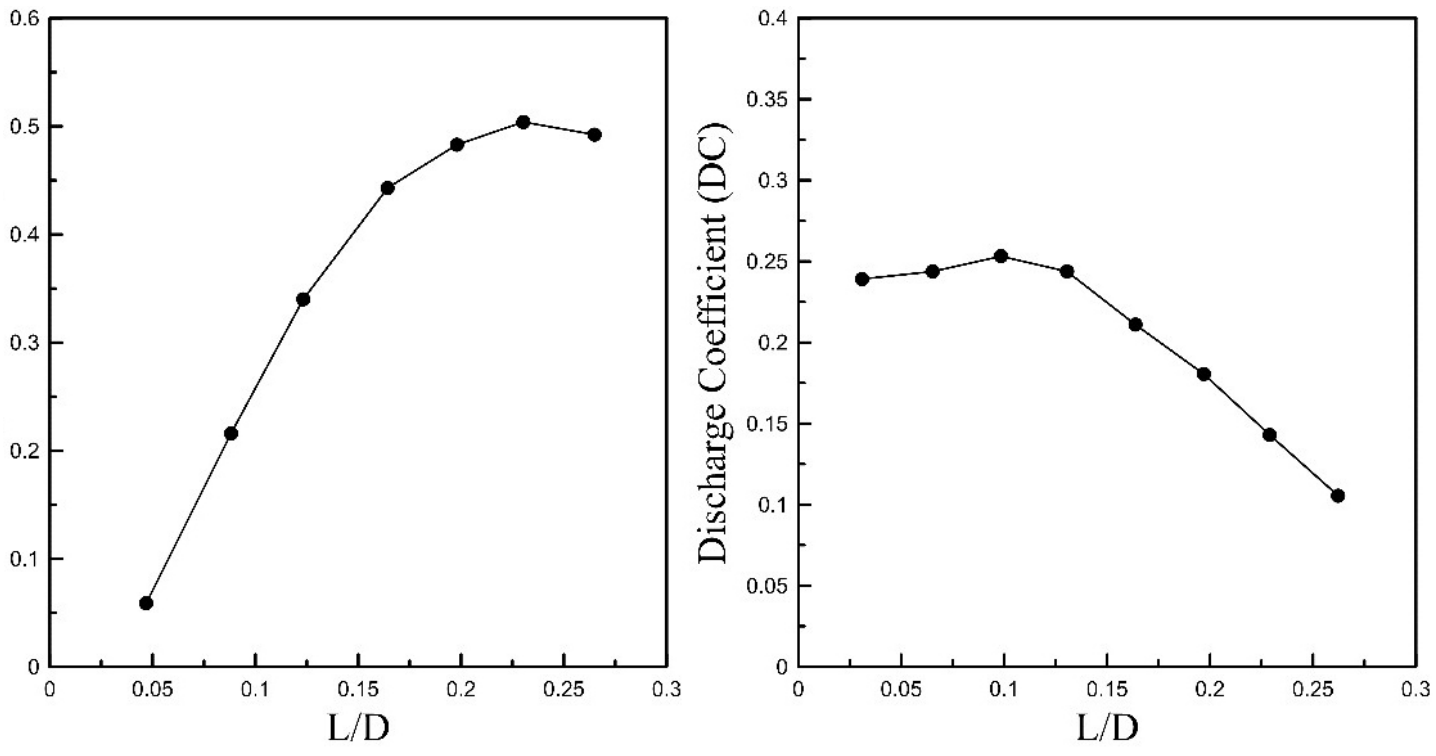

Fig. 8. CD for the a) constant, b) variable reference areas compared to the valve area.
Source: Authors.

During the first valve lift between 0 L/D and 0.14 L/D (Fig. 8a), it can be observed a sharp increase of the CD, which has a proportional relation with the valve lifting. The last behavior can be explained because, in that instant, the CD is completely related to the distance between the head and the bottom of the valve [21]. Therefore, within this interval, the CD increments exponentially for any abrupt distance increment in the valve lifting. Subsequently, when the valve is descending and lifting distance offset 0.14 L/D, the increment of the CD is less substantial as it only varies from 0.4 L/D to 0.5 L/D (Fig. 8a) as it reaches the Bottom Dead Center (BDC) [36]. Additionally, it is worth mentioning that whenever a variable reference area is considered, the overall behavior describes a different curve which present discontinuities along with the valve lifting [23], [35], [36].

For the first valve lift between 0 L/D and 0.1 L/D (Fig. 8b), the overall behavior of the CD is related to the geometry of the distance between the head and the bottom of the valve. Thus, as the airflow is dependent on the valve motion, the real mass flow will grow in the same proportion resulting in higher CD values. When the valve lifting reached 0.12 L/D to 0.17 L/D, the separation between the valve and the intake valve opening area is greater, which reduced the CD value [37].

The separation region becomes greater as the valve lifting distance increased, compensating the increment of the effective area induced by the valve aperture. In general, flow separation from the bottom of the valve occurs as the lifting distance increased, which produces a continuous reduction of the mass flow, as can be noticed for the 0.12 L/D to 0.27 L/D range.

The curves presented in Fig. 8 describe opposite behaviors as they are related to different effective area approaches. Within 0.1 L/D, it can be noticed that the reference area specifies the behavior of the curves. First, the real mass flow rate increments as the valve lifting get larger. However, at this stage, the increment rate becomes less prominent for the variable reference case as shown in Fig. 8b, which experiences a decreasing trend as the impact of the real mass flow increment is not proportional to the area enlargement, generating an increment on the theoretical mass flow rate [5], [23]. In contrast, the curve for the constant area approach remains

with the increasing trend. However, the increment rate decreases with the valve lifting, which produces the logarithmic curve. In fact, as the valve separates from the initial position, the flow velocity decreased, which explained the reason why the curve of CD for the constant area falls as it reaches the end of the valve lifting.

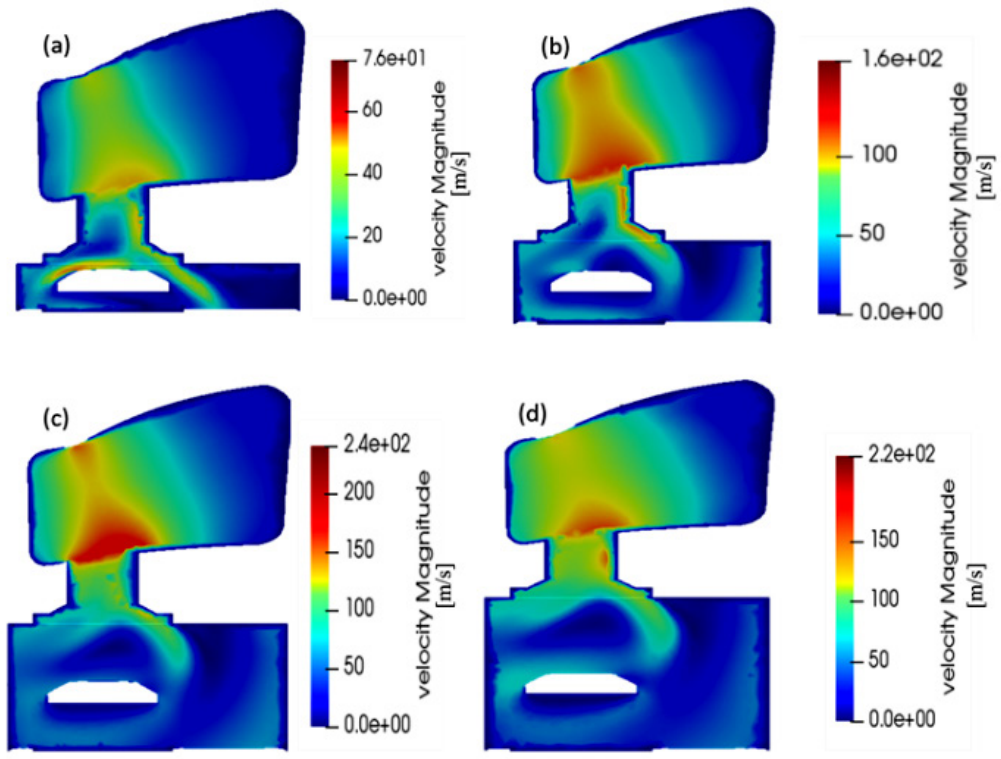

Fig. 9. Velocity profiles close to the head valve region at valve lifting of (a) 2.15 mm, (b) 4.3 mm, (c) 6.45 mm, (d) 8.6 mm.
Source: Authors.

B. *Characterization of swirl coefficient (SC)*

The analysis incorporates 4 different lifting valve distances: 2.15 mm, 4.3 mm, 6.45 mm, and 8.6 mm, to obtain a better visualization of the phenomena [12]. Accordingly, a progressive change can be observed for the velocity vectors, which generates the common vortex flow pattern [5].

As the mass flow rate increments as a function of the rotational regime, the SC changes for each value measured. According to Fig. 10, the SC is not dependent on the mass flow entering the cylinder but depends on the tangential and axial velocities. Thus, it can be noticed that the curves describe a non-linear behavior, obtaining similar patterns for all the valve lifting progressions at 3 000 rpm and 3 800 rpm regimes.

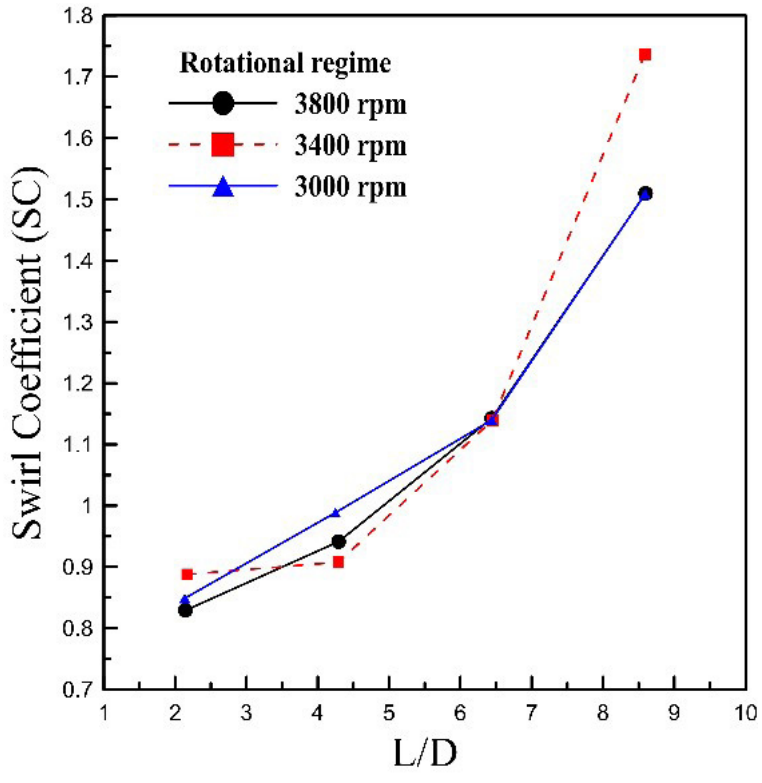

Fig. 10. CT (3 000 rpm-0.9 kg/s) (3 400 rpm-0.01kg/s), (3 800 rpm-0.011 kg/s).
Source: Authors.

C. *Flow at the first stage of admission*

The axial flow during this stage is almost constant inside the cylinder. The majority of velocity vectors contribute to the increment of the SC, which is the expected behavior of single-valve engines. Also, it can be seen that there is no interference of external air jets as experienced in double-valve engines [30], [38]. Hence, the dominant flow generation features a dextro-rotatory pattern to the reference axis.

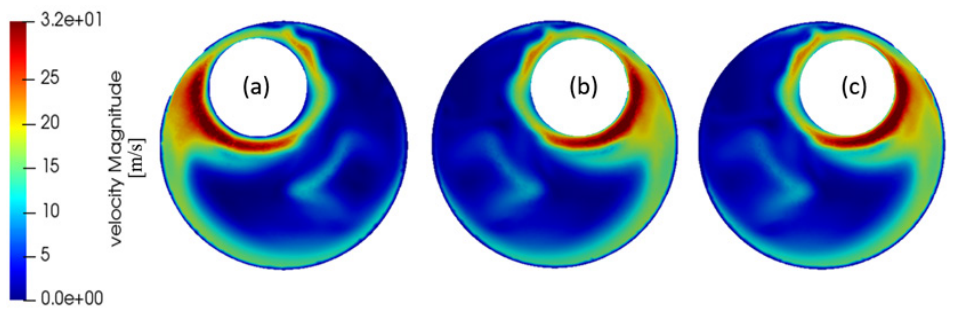

Fig. 11. Tangential velocity profiles in a perpendicular axis to Lv = 2.15 mm, operating at a rotatory regime of (a) 3 000 rpm, (b) 3 400 rpm, (c) 3 800 rpm.
Source: Authors.

D. *Flow at an intermediate stage of admission*

Within the first seconds of admission, the limited distance between the cylinder head and the piston does not allow the swirl flow development, thus its generation stars as the admission process continuous, as can be noticed in the valve lifting distance of 4.3 mm (Fig. 12). The airflow rotation evolves in the upper region, where a unidirectional direction is generated in a perpendicular axis to the cylinder. In addition, a minor region experiences a radial discharge with regards to the valve axis that promotes negative local velocities [39].

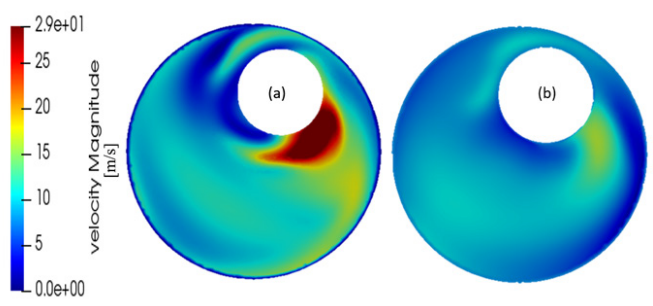

Fig. 12. Tangential velocity profiles in a perpendicular axis to (a) Lv = 4.30 mm and (b) Lv = 6.45 mm, operating at a rotatory regime of 3 000 rpm.
Source: Authors.

On the other hand, when the distance to the cylinder head becomes greater (Lv = 6.45 mm), the air develops a predominant rotation direction, and the velocity vectors indicate that the negative local velocities are considerably reduced while establishing a single vortex as shown in Fig. 13. However, the overall flow behavior differs from the single rigid vortex pattern. Also, irregular velocity profiles with a decentralized vortex center can be observed [40].

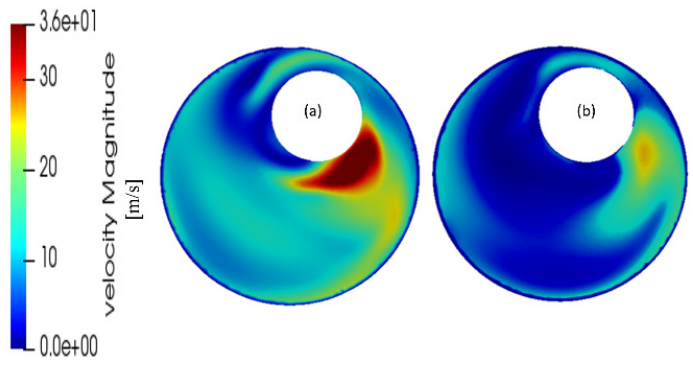

Fig. 13. Tangential velocity profiles in a perpendicular axis to (a) Lv = 4.30 mm and (b) Lv = 6.45 mm, operating at a rotatory regime of 3800 rpm.
Source: Authors.

E. *Flow in the final stage of admission*

In this specific stage (Fig. 14), the valve is almost closing. Additionally, the piston is near the BDC. Therefore, the piston speed is limited, and the inlet velocities are significantly lower than in previous stages. The airflow inside the cylinder features homogenous velocities at the end of the admission. Lastly, it can be seen how the forced vortex with an asymmetric center from the cylinder axis is consolidated [41], [42].

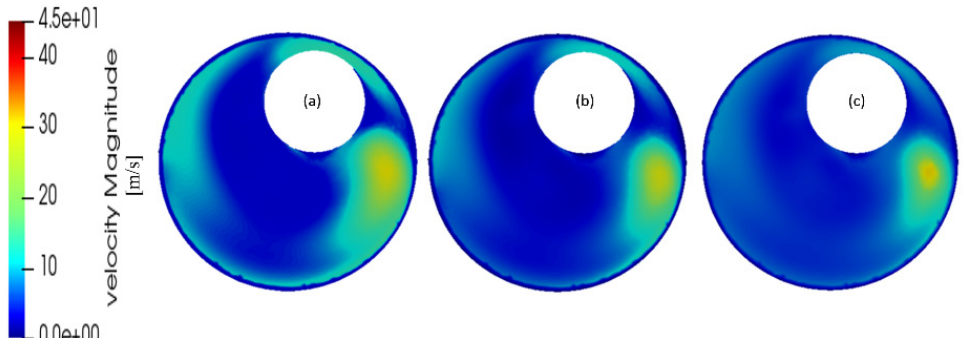

Fig. 14. Tangential velocity profiles in a perpendicular axis to Lv = 8.60 mm, operating at a rotatory regime of (a) 3 000 rpm, (b) 3 400 rpm and (c) 3 800 rpm.
Source: Authors.

VI. Conclusions

The study aimed to analyze the airflow behavior in the intake system of a low-displacement diesel engine F300A. CFD simulations revealed the overall flow patterns and behavior of the intake process. This investigation reinforced the CFD approach as a robust tool to adjust the numerical results with experimental values by incorporating correction factors through similarity laws. This methodology can be extrapolated for other engine applications while reducing up to 15% of the error margin.

From the results, the airflow features a concrete development as the valve lifting distance increments. Also, it was found that the tangential velocity experiences irregularities in the flow stream, producing a decentralized center from the cylinder axis from low to medium valve lifting values. The curves of the cylinder intake showed a clear similarity for both experimental and numerical methodologies. Therefore, it can be concluded that parameters such as the airflow values during intake are not dependent on the rotatory regime.

Even though the DC and SC do not define the airflow completely, it was demonstrated that they provide insightful information for decision-making of the engine intake design, which can be used to reduce the emissions by optimizing the performance of the system. The elevated velocities encountered at the beginning of the admission are related to the cylinder geometry. In the study, the helicoidal valve pipe fosters maximum turbulence flow in the valve´s head before moving downward.

Specifically, the DC is determined by the initial pressure conditions as this parameter experience a direct correlation with the pressure differential. The DC value ranged between 0 L/D to 0.5 L/D for a constant reference area, staying that this cylinder can displace 50% of the theoretical airflow with a valve diameter of 30.5 mm and a chamber volume of 0.3 L. The results are significantly high when compared to the literature values [1], [23], [38] for double-valve intake engines. In contrast, the values of the DC for the variable reference area vary from 0.3 L/D to 0.19 L/D, which indicates that in the worst-case scenario, the engine reduces its airflow displacement by around 11% compared to the ideal capacity.

The tangential velocity within the airflow is determinant in the vortex generation. The results showed that for a rotation regime of 3 000 rpm and 3 400 rpm, a concrete vortex appeared when implementing the methodology of Thien [7]. This pattern can be analyzed in Fig 13. where the values closed to the center zone are close to 0 m/s, whereas the peripheric region features values between 10 m/s to 20 m/s, which support the dextro-rotatory motion of the airflow inside the cylinder.

The overall pattern of the axial velocity showed the ordinary behavior of single-valve intake engines in which the airflow circulates from the head to the bottom of the valve and continues to flow to the walls producing a single vortex. From the numerical results, it can be verified that the

SC reached a maximum value at the end of the valve lifting distance, which indicates that the vorticity is generated before the piston starts the compression stroke. The last pattern is supported by the axial velocity profiles where the single-vortex is produced at the end of the valve lifting stroke. The axial flow experiences toroidal vortex progression where the highest velocities are found in the peripheric zone; meanwhile, the center region experiences lower velocities. For different rotatory regimes, it can be seen that the results remain constant, excepting the 3 400 rpm, which experiments a slight increase. Thus, it can be inferred that at this flow regime, the optimal vorticity generation for the engine is established.

The numerical analysis of the airflow in low-displacement diesel engines is not extensively reviewed, as most investigations focus on high-capacity engines. However, low-displacement engines are widely implemented, which reinforces the relevance of the present study to describe the flow interactions in the combustion process and further promotes high efficiency while reducing emissions.

Acknowledgments

The authors thank the Universidad del Atlántico, Sphere Energy company, and KAI research unit for their support in the development of this investigation by allowing the use of its facilities and the required instrumentation.

References

[1] Y. Varola, H. F. Oztop, M. Firata & A. Kocab, "CFD Modeling of heat transfer and fluid flow inside a pent-roof type combustion," *Int Commun Heat Mass*, vol. 37, no. 9, pp. 1366–1375, Nov. 2010. https://doi.org/10.1016/j.icheatmasstransfer.2010.07.003

[2] S. Jiang, S. Zhu, H. Wen & S. Huang, "Parameter analysis of diesel helical intake port numerical desing," *Energy Procedia*, vol. 16, Part A, pp. 558–563, 2012. https://doi.org/10.1016/j.egypro.2012.01.090

[3] B. Jayashankara & V. Ganesan, "Effect of fuel injection timing and intake pressure on the performance of DI diesel Engine - A parametric study using CFD," *Energy Convers Manag*, vol. 51, no. 10, pp. 1835–1848, 2009. http://dx.doi.org/10.1016/j.enconman.2009.11.006

[4] G. Kalghatgi, "Developments in internal combustion engines and implications for combustion science and future transport fuels," *Proc Combust Inst*, vol. 35, no. 1, pp. 101–115, 2014. https://doi.org/10.1016/j.proci.2014.10.002

[5] A. Gil, *Modelado tridimensional del flujo de aire en el cilindro de motores diesel de inyeccion directa*. VA, ES: Reverte, 2007.

[6] J. S. Meurer, "Die Erzeugung von Drehbewegungen der Luft in den Zylindern schnellaufender Viertakt-Dieselmaschinen durch die Einlaßorgane," *MAN-Forsch*, n. 1, s. 8–22, 1951.

[7] G. Thien, "Entwicklungsarbeiten an ventilkanälen on viertakt Diesel Motoren," *ÖIZ*, vol. 8, n. 9, 1965.

[8] T. Uzkan, C. Borgnakke & T. Morel, "Characterization of Flow produced by a high-swirl inlet port," IHC, AA, MI, USA, *SAE Technical Papers 830266*, 1983. https://doi.org/10.4271/830266

[9] J. Morea-Roy, M. Muñoz & F. Moreno, "Simulación numerica del ciclo operativo de un motor de encendido provocado," *Rev inter met num calc dis ing*, vol. 15, no. 2, pp. 207–216, 1999. Disponible en http://hdl.handle.net/2099/4567

[10] A. Rahiman, A. Razak, M. Samee & M. K. Ramis, "CFD Analysis of flow field development in a direct injection diesel engine with different manifolds," *Am J Fluid Dyn*, vol. 4, no. 3, pp. 102–113, 2014. Available: http://article.sapub.org/10.5923.j.ajfd.20140403.03.html

[11] R. Holkar, Y. N. Sule-Patil, S. M. Pise, Y. A. Godase & V. Jagadale, "Numerical simulation of steady flow through engine intake system using CFD," *IOSR JMCE*, vol. 12, no. 1, pp. 30–45, 2015. Available: https://www.iosrjournals.org/

[12] J. V. Pastor, *Movimiento del aire en motores diesel de inyeccion directa*, VAL, ES: UPV, 1997.

[13] G. Thien, "Derivation of the formulas for the evaluation of stationary flow measurements," ÖIZ, AU, VIE, *AVL-FA-Report N°. 463/Gen./072*, 1978.

[14] G. Thien, "Entwicklungsarbeiten an Ventilkanalen von Viertakt Dieselmotoren," *ÖIZ*, vol. 9, 1965.

[15] J. C. Dent & J. A. Derham, "Air Motion in a Four-Stroke Direct Injection Diesel Engine," *IME*, vol. 188, no. 21, pp. 269–280, Jun. 1974. https://doi.org/10.1243%2FPIME_PROC_1974_188_030_02

[16] G. C. Davis & J. C. Kent, "Comparison of model calculations and experimental measurements of the bulk cylinder flow processes in a motored PROCO engine," SAE, DET, USA, *SAE Technical Paper 790290*, 1979. https://doi.org/10.4271/790290

[17] R. C. Engineers, "Information to clients on Ricardo's Laser-Doppler velocimeter," *Ricardo Engineering Report*, 1976.

[18] A. Murakami, M. Arai & H. Hiroyasu, "Swirl Measurements and Modelling in Direct Injection Diesel Engines," Univ Hiroshima, HIJ, JPN, *SAE Technical Paper 880385*, 1988. https://doi.org/10.4271/880385

[19] R. Leal & J. L. Filgueiras, "Industrial airflows numerical simulation in ducts and devices using all-speed algorithm in structured meshes," *Ingeniare*, vol. 26, no. 2, pp. 273–282, 2008. http://dx.doi.org/10.4067/S0718-33052018000200273

[20] L. Rodríguez, M. Collado, E. Rodríguez & L. Patiño, "Análisis numérico del comportamiento del aire en un sistema de distribución de aire acondicionado empleando los modelos de turbulencia K-E, RNG K-E y el modelo de las tensiones de Reynolds," *Ingeniare*, vol. 16, no. 2, pp. 370–382, 2008. http://dx.doi.org/10.4067/S0718-33052008000200012

[21] G. P. Blair, H. B. Lau, A. Cartwright, B. D. Raghunathan & D. O. Mackey, "Coefficients of Discharge at the Aperatures of Engines," *J Engines*, vol. 104, no. 3, pp. 2048–2062, 1995. https://doi.org/10.4271/952138

[22] J. Derham, "Air Motion in a Four Stroke Direct Injection Diesel Engine," *Doctoral Thesis*, LUT, Loughb, ENG, 1971. Available: https://hdl.handle.net/2134/36161

[23] H. Fujimoto, T. Nakagawa, H. Kudo, T. Wakisaka & Y. Shimamotoc, "A study on the formation of vertical vortex in the cylinder of an I.C engine using CFD: Effect of intake valve closing timing," *JSAE* , vol. 16, no. 4, pp. 349–355, 1995. https://doi.org/10.1016/0389-4304(95)00041-5

[24] J. Benajes, X. Margot, J. Pastor & A. Gil, "Three dimensional calculation of the flow in a DI Diesel engine with variable swirl PORTS," ATTCE, BCN, ES, *SAE Technical Paper 2001-01-3230*, 2001. https://doi.org/10.4271/2001-01-3230

[25] S. Zirngibl, M. Prager & G. Wachtmeister, "Experimental and Simulative Approaches for the determination of the discharge coefficients for inlet and exhaust valves and ports in internal combustion engines," presented *SAE World Congress Experience*, WCX™ 17, DET, USA, 2017. http://dx.doi.org/10.4271/2017-01-5022

[26] S. F. Wang & B. E. Milton, "Investigation of the Helical Inlet Port," presented in *International Fall Fuels and Lubricants Meeting and Exposition*, TIB, TLS, USA, Oct. 13-16, 1997. https://doi.org/10.4271/982539

[27] G. M. Bianchi, G. Cantore & S. Fontanesi, "Turbulence Modelling in CFD Simulation of ICE Intake Flows: The Discharge Coefficient Prediction," *J Engines*, vol. 111, sec. 3, pp. 1901–1918, 2002. http://dx.doi.org/10.4271/2002-01-1118

[28] G. Tippelmann, "A new method of investigation of swirl ports," *SAE Transactions*, vol. 86, sec. 3, pp. 1745–1757, 1977. https://doi.org/10.4271/770404

[29] L. Stager & R. Reitz, presented in "Assessment of Diesel Engine Size-Scaling Relationships," *SAE World Congress*, UW, DET, USA, 16-19 Apr. 2007. https://doi.org/10.4271/2007-01-0127

[30] Ignacio Gómez IHM , "Motores," *igihm.com*. Available: https://www.igihm.com/motores/ (accessed aug. 12, 2019).

[31] P. Stephenson & C. Rutland, "Modeling the Effects of Valve Lift Profile on Intake Flow and Emissions Behavior in a DI Diesel Engine," *Fuels and Lubricants Meeting and Exhibition*, SAE, TOR, CA, 16-19 Oct. 1995. https://doi.org/10.4271/952430

[32] F. Payri, J. Benajes, X. Margot & A. Gil, "CFD modeling of the in-cylinder flow in direct-injection Diesel engines," *Comput Fluids*, vol. 33, no. 8, pp. 995–1021, Sep. 2004. https://doi.org/10.1016/j.compfluid.2003.09.003

[33] A. M. Bharadwaj, K. Madhu, K. J. Seemanthini, K. G. Vismay, T. Aravind & A. M. Shivapuji, "Study of Swirl and Tumble Motion using CFD," *IJTRME*, vol. 1, no. 2, pp. 5–8, 2013. Available from http://www.irdindia.in/journal_ijtarme/pdf/vol1_iss2/2.pdf

[34] L. Staples, R. Reitz & C. Hergart, "An Experimental Investigation into Diesel Engine Size-Scaling Parameters," *SAE Int J Engines*, vol. 2, no. 1, pp. 1068–1084 , 2009. https://doi.org/10.4271/2009-01-1124

[35] Y. Shi & R. Reitz, "Study of Diesel Engine Size-Scaling Relationships Based on Turbulence and Chemistry Scales," *SAE World Congress & Exhibition*, SAE, DET, USA, p. 1–21, 14-17 Apr. 2008. https://doi.org/10.4271/2008-01-0955

[36] M. Tess, C. Lee & R. Reitz, "Diesel Engine Size Scaling at Medium Load without EGR," *SAE Int. J. Engines*, vol. 1, no. 1, pp. 1993–2009, 2011. https://doi.org/10.4271/2011-01-1384

[37] M. Masi, L. Artico & P. Gobbato, "Measurements of the Intake and In-Cylinder Flow Field to investigate the reliability of CFD Steady-state simulation for actual engines," *12th International Conference on Engines & Vehicles*, SAE, Capri, IT, 13-17 Sept. 2015. https://doi.org/10.4271/2015-24-2404

[38] X. Yang, T.-W. Kuo, O. Guralp, R. O. Grover & P. Najt, "In-Cylinder Flow Correlations between steady flow bench and motored engine using computational fluid dynamics," *J Eng Gas Turbine Power J Eng Gas Turb Power*, vol. 139, no. 7, pp. 1–8, 2017. https://doi.org/10.1115/1.4035627

[39] B. V. V. S. U. Prasad, C. S. Sharma, T. N. C. Anand & R. V. Ravikrishna, "High swirl-inducing piston bowls in small diesel engines for emission reduction," *Applied Energy*, vol. 88, no. 7, pp. 2355–2367, 2011. https://doi.org/10.1016/j.apenergy.2010.12.068

[40] M. Battistoni, A. Cancellieri & F. Mariani, "Steady and Transient Fluid Dynamic Analysis of the tumble and swirl evolution on a 4V engine with independent intake valves action," *PF&L Meeting*, SAE, RSMT, USA, 6-9 Oct. 2008. https://doi.org/10.4271/2008-01-2392

[41] A. A. E.-S. Mohamed, S. Abo-Elfadl, A. E.-M. M. Nassib, "*Effect of shroud and orientation angles of inlet valve on flow characteristic through helical-spiral inlet port in diesel engine*," *J. Eng. Gas Turbines Power*, vol. 139, no. 10, pp. 1–7, Oct. 2017. https://doi.org/10.1115/1.4036381

[42] E. Barrientos, I. Bortel, M. Takats & J. Vavra, "Impact of intake induced swirl on combustion and emissions on a single cylinder diesel engine," *ICEF*, ASME, GRVL, USA, 9–12 Oct. 2016. http://dx.doi.org/10.1115/ICEF2016-9325

Carlos Santos. Universidad del Atlántico (Colombia). https://orcid.org/0000-0002-6063-297X

Luís Pérez. Universidad del Atlántico (Colombia). https://orcid.org/0000-0003-1555-8843

Jorge Duarte. Universidad del Atlántico (Colombia). https://orcid.org/0000-0001-7345-9590